JYX JYVÄSKYLÄN YLIOPISTO UNIVERSITY OF JYVÄSKYLÄ

**This is a self-archived version of an original article. This version may differ from the original in pagination and typographic details.**

**Author(s):** Mäkelä, Eveliina; Lahti, Riikka; Jaatinen, Salla; Romar, Henrik; Hu, Tao; Puurunen, Riikka L.; Lassi, Ulla; Karinen, Reetta

**Title:** Study of Ni, Pt, and Ru Catalysts on Wood-based Activated Carbon Supports and their Activity in Furfural Conversion to 2-Methylfuran

**Year:** 2018

**Version:** Accepted version (Final draft)

**Copyright:** © 2018 Wiley-VCH Verlag GmbH & Co. KGaA, Weinheim

**Rights:** In Copyright

**Rights url:** http://rightsstatements.org/page/InC/1.0/?language=en

**Please cite the original version:**

Mäkelä, E., Lahti, R., Jaatinen, S., Romar, H., Hu, T., Puurunen, R. L., Lassi, U., & Karinen, R. (2018). Study of Ni, Pt, and Ru Catalysts on Wood-based Activated Carbon Supports and their Activity in Furfural Conversion to 2-Methylfuran. ChemCatChem, 10(15), 3269-3283. https://doi.org/10.1002/cctc.201800263

# Study of Ni, Pt and Ru catalysts on wood-based activated carbon supports and their activity in furfural conversion to 2-methylfuran

Eveliina Mäkelä,*[a] Riikka Lahti,[b][c] Salla Jaatinen,[a] Henrik Romar,[b][c] Tao Hu,[c] Riikka L. Puurunen,[a] Ulla Lassi,[b][c] and Reetta Karinen[a]

**Abstract:** Bio-based chemicals can be produced from furfural through hydrotreatment. In this study, 2-methylfuran (MF), a potential biofuel component, was produced with Pt, Ru and Ni catalysts supported on wood-based activated carbons. The catalytic hydrotreatment experiments were conducted in a batch reactor at 210-240 °C with 2-propanol as a solvent and 40 bar $H_2$ pressure. Two types of activated carbon supports were prepared by carbonization and activation of lignocellulosic biomass (forest-residue-based birch and spruce from Finland). Both types of activated carbons were suitable as catalysts supports giving up to 100% furfural conversions. The most important factors affecting the MF yield were the metal dispersion and particle size as well as reaction temperature. The highest observed MF yields were achieved with the noble metal catalysts with the highest dispersions at 240 °C after 120 min reaction time: 3 wt.% Pt on spruce (MF yield of 50%) and 3 wt.% Ru on birch (MF yield of 49%). Nickel catalysts were less active most likely due to lower dispersions and incomplete metal reduction. Interesting results were obtained also with varying metal loadings: the lower Pt loading (1.5 wt.%) achieved almost the same MF yield as the 3 wt.% catalysts which can enable the production of MF with high yields and reduced catalyst costs. Based on this study, biomass-based renewable activated carbons can be used as a catalyst supports in furfural hydrotreatment with high conversions.

## Introduction

Due to increasing global energy demand and the concerns related to the biofuels produced from edible crops or starch, lignocellulosic biomass is becoming an attractive option to replace fossil-based fuels and chemicals.[1–3] Furfural is a biomass-derived platform chemical, which can be upgraded to several valuable products using hydrotreatment[4] (Scheme 1), such as furfuryl alcohol (FA), 2-methylfuran (MF), tetrahydrofurfuryl alcohol (THFA), 2-methyltetrahydrofuran (MTHF), furan, 2-pentanone (PN) and 2-pentanol (POL).

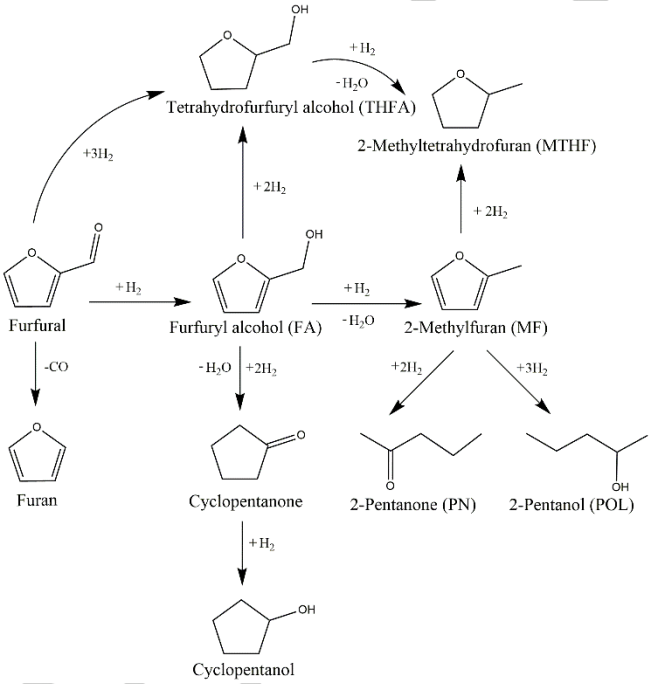


**Scheme 1.** Furfural reaction pathways to 2-methylfuran and other valuable products.

Out of the above-mentioned chemicals, furfuryl alcohol, THFA and 2-methylfuran are currently the most important and widely utilized in chemical industry.[5,6] 2-Methylfuran is known for its solvent properties that are similar to other widely utilized solvents, such as furan and tetrahydrofuran. Recently, MF has been considered as a potential biofuel component that can be blended with gasoline.[6] The heating value of MF (28.5 MJ $l^{-1}$) is close to gasoline and 35 % higher than that of ethanol.[7] The octane number for MF (RON 131) is high and the water solubility (7 g $l^{-1}$) is low.[8] It also has a lower boiling point (63 °C) than ethanol or gasoline, thus promoting engine stability at low temperatures. Moreover, the high energy density and octane number lead to better resistance to engine knock at higher compression ratios.[7] The combustion of MF together with gasoline has been reported by various authors.[7,9–11] Wei et al.[11] investigated the combustion of MF blended to gasoline and found lower hydrocarbon and carbon monoxide emissions compared to pure gasoline. Recently, the blending of MF with diesel fuel was

[a] E. Mäkelä,* S. Jaatinen, Prof. R. L. Puurunen, Dr. R. Karinen
Department of Chemical and Metallurgical Engineering
Aalto University
P.O. Box 16100, 00076 AALTO, Finland
E-mail: eveliina.makela@aalto.fi
[b] R. Lahti, Dr. H. Romar, Dr. T. Hu, Prof. U. Lassi
Department of Chemistry
University of Oulu
P.O. Box 3000, 90014 Oulu, Finland
[c] R. Lahti, Dr. H. Romar, Prof. U. Lassi
Kokkola University Consortium Chydenius
University of Jyväskylä
P.O. Box 567, 67101 Kokkola, Finland

Supporting information for this article is given via a link at the end of the document.

investigated by Xiao et al,[12] who reported higher brake thermal efficiency (BTE) for diesel-MF blends than for pure diesel. However, the $NO_x$ emissions were reported to increase with increasing the MF fraction in the blend, but the soot emissions were significantly lower compared to pure diesel fuel.[12]

Furfural hydrotreatment studies have been numerous but focused mainly on the production of furfuryl alcohol.[13–17] When low reaction temperatures (80-150 °C) are utilized, Ni and Pt are typically active in hydrogenation leading to furfuryl alcohol as the main product.[16,18,19] At high temperatures (≥ 230 °C), the decarbonylation towards furan dominates.[20] Recently, the production of also MF from furfural has been studied.[8,21] The production of MF is preferred via hydrogenolysis since it removes the oxygen while maintaining the carbon number unchanged.[8] Although the majority of the research has focused on gas phase hydrotreatments,[22] liquid phase upgrading can be preferred due to the compatibility with furfural production process.[23,24] The effect of Ni, Pt and Ru catalysts and various solvents were investigated by Hronec et al.[25,26] and Ordomsky et al.[27] The authors discovered that while the same catalysts catalyze hydrogenation or decarbonylation in alcohol media, furan ring rearrangement is preferred leading to cyclopentanone and cyclopentanol when the solvent is water. Various furfural hydrotreatment studies were listed by Yan et al.[6], and 2-propanol was among the most widely used solvents in this reaction. Alcohols in general are good solvents as furfural is soluble in them.

Thus far, the most common furfural hydrotreatment catalyst has been copper chromite.[6] However, the environmental regulations have directed the catalyst development from chromium to more harmless metals, such as Ni and noble metals.[22] The majority of the studied noble metal and Ni catalysts have been commercial or prepared on commercial activated carbon supports: Ru/C,[23,25,27–30] Pt/C,[25,30,31] Pd/C[25,30,32] and Ni/C.[22,33] However, little is known about the effect of the structure of activated carbon (AC) on furfural hydrotreatment. Activated carbons are known to have large specific surface area, well-developed highly porous structure, chemical and physical stability and surface functionality influencing the surface characteristics and adsorption behavior.[34–37] ACs have many attractive properties that can affect the preparation of supported metal catalysts. Carbon support can be tailored for a specific reaction with physical or chemical treatment before, during or after the activation.[34,36] The carbon surface groups containing heteroatoms, such as oxygen, can act as anchoring sites for metal particles and generate high metal dispersion.[34] Carbon support can ease the reduction of metal by having a weaker metal-support interaction compared to conventional oxide supports.[34,37] The precious metal phase can be further recovered by burning away the carbon support.[34] Most of the AC, almost 60% on the market, is produced from coal-based materials including bituminous coal and lignite.[38] Due to the growing demand of ACs (11% annual growth[39]) and the environmental aspects, biobased carbons have received attention. Attractively, ACs can be prepared from residual and waste biomass, which are renewable materials and could decrease the "carbon footprint" of a biomass transformation process.[36,40,41]

In this study, we investigated the structure and composition of two types of activated carbon prepared from lignocellulosic biomass residue from Finnish birch and spruce. Further, we used these materials in catalytic furfural hydrotreatment in the liquid phase with a goal to produce MF with high yield.

## Results and discussion

### Characterization of the AC supports and fresh catalysts

#### *Chemical composition*

The chemical composition of the supports was analyzed with elemental, total carbon (TC) and ash content analysis (Table 1). The total carbon content was higher for spruce-based activated carbon (AC-S) than for birch-based activated carbon (AC-B). On the basis of the elemental analysis (C, H, N, O, S), AC-B had higher content of oxygen than AC-S. Hydrogen and nitrogen contents were almost the same for both supports and no sulfur was detected. Ash content (inorganic material) was higher for the birch-based than for the spruce-based AC (7.9 wt.% and 2.6 wt.% respectively). Overall, the inorganic materials in the prepared supports were low when compared to the commercial ACs, in which the ash content can be as high as 10–15 wt.%.[34]

**Table 1.** Total carbon (TC), inorganic content (ash) and elemental analysis results of the organic part (C, H, N, O, S) of AC-S and AC-B.

| Sample | TC /wt.% | Ash /wt.% | Elemental analysis /wt.% C | H | N | O | S |
|---|---|---|---|---|---|---|---|
| AC-S | 92.3 | 2.6 | 90.8 | 0.7 | 0.8 | 2.1 | 0.0 |
| AC-B | 86.8 | 7.9 | 82.6 | 0.7 | 0.6 | 3.5 | 0.0 |

Metal contents of the ACs were measured by inductively coupled optical emission spectrometry (ICP-OES). Both AC supports contained K, Ca and Mg (Table 2). The birch-based support also contained Na, but for the spruce-based support, the amount of Na was below the detection level. AC-S contained less impurity metals than the birch-based support, and the most abundant impurity metals were potassium and calcium. There might be some interference of these metals, especially K and Ca, as basic promotors in catalysis.[42] Potassium has been acknowledged for its ability to oxidize carbon.[43] It can be used as a catalyst in carbon oxidation purposes (typically in the form of potassium carbonate), such as gasification or exhaust gas clean-up.[43,44] K promotion has also been used to increase catalyst's activity in reverse water gas shift reaction (hydrogenating of $CO_2$) followed by Fisher-Tropsch synthesis.[45] A number of other metals including Zn, Cr, Fe, Ni, Pb and Cu were less than 0.01 wt.%.

The nominal active metal contents in the supported catalysts were 1.5, 3 or 10 wt.%. The measured metal contents of

**Table 2.** ICP measurement results of K, Na, Ca and Mg in AC supports and in impregnated fresh catalysts, and active metals (Pt, Ru and Ni) in fresh and spent catalysts (hydrotreatment at 230 °C) with the target metal contents indicated.

| Sample | K /wt.% | Na /wt.% | Ca /wt.% | Mg /wt.% | Pt /wt.% | Ru /wt.% | Ni /wt.% |
|---|---|---|---|---|---|---|---|
| AC-S | 0.25 | <0.01 | 0.42 | 0.06 | | | |
| AC-B | 1.7 | 0.04 | 0.64 | 0.18 | | | |
| 1.5Pt/AC-S | <0.50 | <0.01 | 0.49 | 0.08 | 1.2 | | |
| 3Pt/AC-S | <0.50 | <0.01 | 0.40 | 0.07 | 2.3 | | |
| 3Pt/AC-B | 0.83 | 0.06 | 0.42 | 0.10 | 3.2 | | |
| 1.5Ru/AC-B | 0.93 | <0.01 | 0.36 | 0.10 | | 1.7 | |
| 3Ru/AC-S | 0.38 | 0.06 | 0.51 | 0.07 | | 2.8 | |
| 3Ru/AC-B | 0.68 | 0.05 | 0.45 | 0.11 | | 2.9 | |
| 3Ni/AC-S | 0.29 | <0.01 | 1.10 | 0.16 | | | 2.0 |
| 3Ni/AC-B | 0.60 | 0.05 | 0.45 | 0.10 | | | 2.5 |
| 10Ni/AC-S | 0.40 | <0.01 | 0.49 | 0.07 | | | 8.9 |
| 3Pt/AC-S spent | | | | | 2.1 | | |
| 3Ru/AC-B spent | | | | | | 0.84 | |
| 3Ni/AC-S spent | | | | | | | 1.7 |

the impregnated catalysts were close to the nominal values with 3Ru/AC-S, 3Ru/AC-B and 3Pt/AC-B catalysts. However, the amount of nickel in the catalysts and platinum in spruce-based catalysts were lower than expected. Most likely, some metal was lost in the impregnation step. When the interaction between the support and the precursor metal is weak, the metal might be transported to the external surface during the drying step.[46] Point of zero charge (PZC) was determined to be around 10 for both supports. In our impregnation solution, the pH was below 10, and the AC surface was positively charged. Interestingly, the impregnated metal content was in all cases higher on birch-based than spruce-based support. This could be due to the higher oxygen content since the oxygen containing functional groups are in many cases related to the adsorption of metal cations.[46,47]

### *Adsorption tests with dye molecules*

Adsorption tests with Methylene blue (MB, basic dye) and Orange II (OR, acidic dye) were performed for AC supports. Information on the adsorption of large molecules (MB and OR dye), that cannot fit onto micropores, is especially important when large molecules need to adsorb onto the pores of AC during the reaction. Adsorption tests can also be used to detect surface functionality.[48,49]

The results from the adsorption tests are presented in Table 3. AC-B removed about 90% of the dyes and AC-S about 80% indicating that the surfaces of both AC were highly mesoporous. The removal of the cationic dye (MB) was more efficient than the removal of the anionic dye (OR). Overall, the birch-based support had better removal of dyes, indicating higher total amount of charged functional groups on the surface.[50]

**Table 3.** Adsorption of Methylene blue (MB) and Orange II (OR) onto activated carbons prepared from birch or spruce.

| Sample | OR adsorption /% | OR adsorption /mg $g^{-1}$ | MB adsorption /% | MB adsorption /mg $g^{-1}$ |
|---|---|---|---|---|
| AC-S | 75 | 250 | 83 | 272 |
| AC-B | 90 | 294 | 93 | 305 |

### *Electron microscopy*

The morphology of the thermally treated, unreduced catalyst particles was studied with a field emission scanning electron microscope (FESEM) and an energy filtered transmission electron microscope (EFTEM). SEM images for thermally treated, unreduced 3Pt/AC-S catalyst (Figure 1a and b) reveal that the active metal particles were evenly distributed on the surface. SEM images of the 3Ru/AC-S catalyst (Fig. 1c and d) showed typical water transportation holes in the wood structure, found to be present in all samples. In some images taken from the Ru catalyst, also larger metal particles were present on the surface of the support. SEM images from the 3Ni/AC-S catalyst (Fig. 1e and f) showed that some metal particles were present as larger "chips"; however, also smaller particles were present.

TEM images (Figure 2) showed that Pt particles were quite evenly distributed on the catalyst surface. Pt particle sizes were estimated to be in the range of 5–10 nm for 3 wt.% catalysts. The Pt particles on birch-based support were slightly larger than particles on spruce-based support. The Pt particle size of 3–20 nm was estimated for the 1.5 wt.% catalyst with more variety in

WILEY-VCH

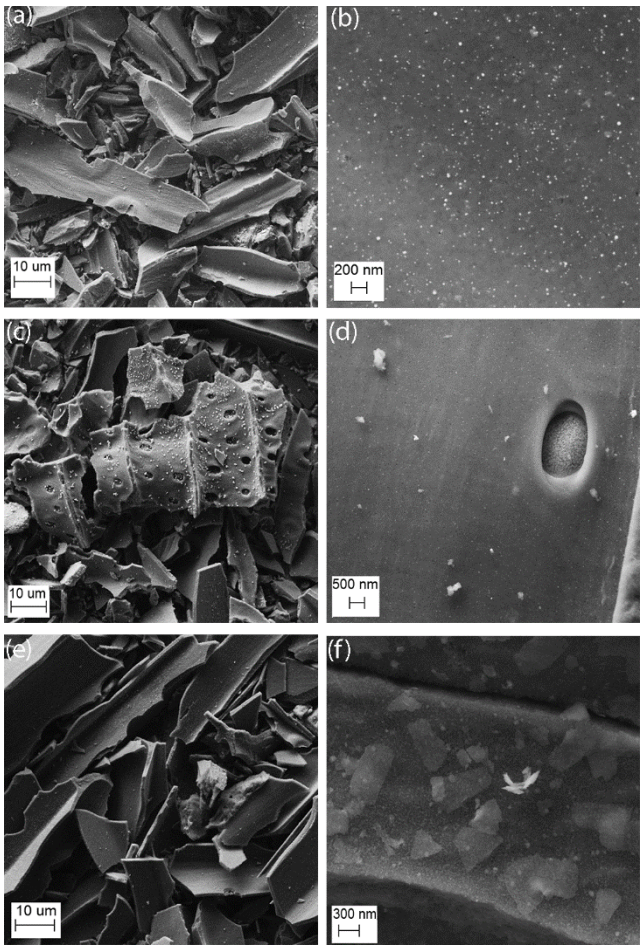


**Figure 1.** SEM images from fresh, thermally treated catalysts on spruce derived AC. (a) and (b) 3Pt/AC-S, (c) and (d) 3Ru/AC-S, (e) and (f) 3Ni/AC-S. The metal particles are shown as bright dots or other shapes on the support surface. Note that the close-up figures differ in scale.

size than with the 3 wt.% catalysts. Metal particles in all Ru catalysts were less than 5 nm and appeared evenly distributed on the surface. TEM images taken from the 3Ni/AC-B catalyst showed the presence of some larger metal clusters, over 20 nm diameter, which were further analyzed with an energy dispersive X-ray spectroscopy (EDS) to be nickel-calcium aggregates. For 3Ni/AC-S catalyst, TEM images showed smaller particle size (less than 10 nm), and for 10Ni/AC-S, particle size of ca. 10 nm.

### *Physisorption analysis*

Specific BET surface areas (SA), average pore diameters, pore volumes and pore size distributions of the prepared AC supports and impregnated catalysts were calculated from nitrogen adsorption isotherms by BET (Brunauer-Emmet-Teller)[51] and DFT (Density Functional Theory)[52,53] methods (Table 4). AC-S and AC-B both had BET surface areas over 1000 $m^2$ $g^{-1}$, which are well comparable with commercial activated carbons with typical surface areas of 700-1500 $m^2$ $g^{-1}$. The pore volumes were ca. 0.7 $cm^3$ $g^{-1}$ with mesopore (2-50 nm) volumes of ca. 0.35 $cm^3$ $g^{-1}$. According to the DFT method, the mesopore volumes were close to 55% of the total pore volume and expected to be suitable

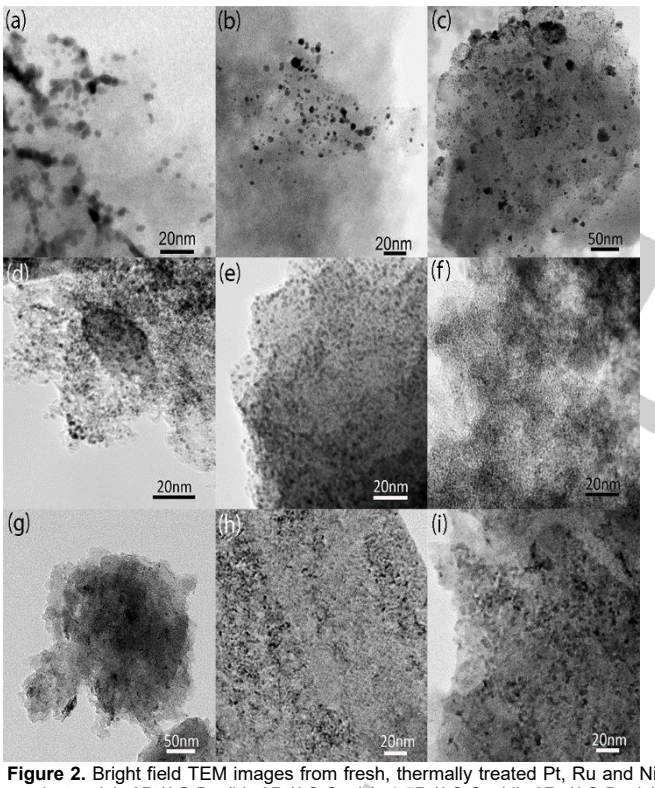


**Figure 2.** Bright field TEM images from fresh, thermally treated Pt, Ru and Ni catalysts: (a) 3Pt/AC-B, (b) 3Pt/AC-S, (c) 1.5Pt/AC-S, (d) 3Ru/AC-B, (e) 3Ru/AC-S, (f) 1.5Ru/AC-B, (g) 3Ni/AC-B, (h) 3Ni/AC-S, (i) 10Ni/AC-S. The metal particles are shown as dark dots.

for a catalyst support. Average pore diameters of ca. 2.8 nm were calculated for the activated carbon supports. Mesoporous structure of the support is preferred in heterogeneous catalysis, since small micropores may not be available for precursors or reactants limiting the effectiveness of the microporosity.[37]

The BET surface areas and average pore volumes decreased typically by 15-25% during the impregnation of metal (Pt, Ru or Ni) on the activated carbon (Table 4). This might be due to the adsorption of metal particles into the pores or partial blocking of the pores. The 3 wt.% Ni catalysts maintained the highest surface areas after impregnation as the surface areas decreased less than 10%. This might indicate that nickel particles were located in the larger pores. As expected with the 10 wt.% catalyst, the surface area and pore volume decreased more (SA ca. 31% and pore volume ca. 44%) than with other catalysts. Overall, the pore volume decrease for other than the 10 wt.% catalyst were in the typical range (ca. 30%) for impregnated catalysts.[54]

### *Chemisorption analysis*

Chemisorption of hydrogen or carbon monoxide on the thermally treated, reduced catalysts was studied to reveal the active metal surface area and dispersion. Based on the analysis, particle sizes for each catalysts were calculated assuming spherical particles and utilizing measured metal loadings. For Pt catalysts, CO was selected as the gas for chemisorption in order to avoid possible

**Table 4.** Summary of the physisorption and chemisorption analysis of the activated carbon supports, and the fresh and spent (230 °C) Pt, Ru and Ni catalysts. The measured metal contents (Table 2) were used in calculating metal dispersion and particle size by chemisorption analysis.

| | **Physisorption** | | | | | | | **Chemisorption** | | |
|---|---|---|---|---|---|---|---|---|---|---|
| Sample | BET SA /$m^2 g^{-1}$ | Pore volume /$cm^3 g^{-1}$ | Average pore diameter /nm | Micro-pores /$cm^3 g^{-1}$ | Meso-pores /$cm^3 g^{-1}$ | Macro-pores /$cm^3 g^{-1}$ | Total volume /$cm^3 g^{-1}$ | Metal SA/ $m^2 g^{-1}$ | Disper-sion /% | Average particle size /nm |
| AC-S | 1010 | 0.71 | 2.8 | 0.28 | 0.34 | 0.00 | 0.62 | | | |
| AC-B | 1050 | 0.75 | 2.9 | 0.29 | 0.35 | 0.00 | 0.64 | | | |
| 1.5Pt/AC-S | 850 | 0.53 | 2.5 | 0.25 | 0.21 | 0.00 | 0.46 | 1.1[a] | 33[a] | 3.1[a] |
| 3Pt/AC-S | 840 | 0.54 | 2.6 | 0.24 | 0.19 | 0.00 | 0.44 | 2.4[a] | 37[a] | 2.7[a] |
| 3Pt/AC-B | 780 | 0.55 | 2.8 | 0.22 | 0.25 | 0.00 | 0.47 | 1.6[a] | 19[a] | 4.8[a] |
| 1.5Ru/AC-B | 870 | 0.61 | 2.8 | 0.24 | 0.27 | 0.00 | 0.51 | 1.8[b] | 20[b] | 4.6[b] |
| 3Ru/AC-S | 770 | 0.46 | 2.4 | 0.23 | 0.17 | 0.00 | 0.40 | 3.3[b] | 22[b] | 4.1[b] |
| 3Ru/AC-B | 880 | 0.62 | 2.8 | 0.25 | 0.28 | 0.01 | 0.53 | 4.3[b] | 26[b] | 3.4[b] |
| 3Ni/AC-S | 910 | 0.63 | 2.8 | 0.26 | 0.29 | 0.00 | 0.55 | 1.6[c] | 12[c] | 8.4[c] |
| 3Ni/AC-B | 990 | 0.67 | 2.7 | 0.27 | 0.30 | 0.00 | 0.58 | 1.2[c] | 7.2[c] | 14[c] |
| 10Ni/AC-S | 690 | 0.40 | 2.3 | 0.21 | 0.13 | 0.00 | 0.34 | 3.0[c] | 7.0[c] | 15[c] |
| 3Pt/AC-S spent | 500 | 0.41 | 3.3 | 0.13 | 0.23 | 0.00 | 0.37 | n.d. | n.d. | n.d. |
| 3Ru/AC-B spent | 270 | 0.25 | 3.7 | 0.06 | 0.16 | 0.00 | 0.22 | n.d. | n.d. | n.d. |
| 3Ni/AC-S spent | 110 | 0.15 | 5.2 | 0.01 | 0.12 | 0.01 | 0.14 | n.d. | n.d. | n.d. |

[a] Reduction: 250 °C, 2h, hydrogen flow; degassing 250 °C, 2h; analysis: 35°C with CO.
[b] Reduction: 350 °C, 2h, hydrogen flow; degassing: 350 °C, 2h; analysis: 75 °C with $H_2$.
[c] Reduction: 350 °C, 2h, hydrogen flow; degassing: 350 °C, 2h; analysis: 35 °C with $H_2$.

distortion of the results by $H_2$ spill over.[55] $H_2$ was used for Ni catalysts in order to avoid the formation of volatile nickel carbonyl compounds during the measurement.[56] The measurement temperature for Pt and Ni was 35 °C. Ru catalysts were analyzed with hydrogen and at a higher temperature (75 °C) as suggested by Shen et al.[57] Examples of the measured isotherms are presented in Supporting Information.

The noble metal catalysts exhibited higher metal dispersions than the nickel catalysts: the best obtained dispersion was 37%for the 3Pt/AC-S catalyst (Table 4). For comparison, a commercial 1 wt.% Pt/AC catalyst (Degussa type F 103 R) was analyzed with CO chemisorption. The Pt metal dispersion obtained for the commercial catalyst was 28%, which lead to the conclusion that prepared catalysts were comparable with the commercial Pt catalyst. For Ru catalysts, the highest obtained dispersion was 26% for 3Ru/AC-B which also had the highest metal surface area (4.3 $m^2 g^{-1}$). For Ni catalysts, the dispersions were lower compared to noble metal catalysts. Compared to the commercial catalysts presented in the literature, the obtained dispersions seemed to be quite typical for Pt, Ru and Ni catalysts on AC supports.[54,58,59]

### *X-ray diffraction*

X-ray diffraction (XRD) was used to analyze the metal phases in the impregnated catalysts. Measurements were performed on thermally treated, unreduced samples. In the X-ray diffractograms (Figure 3), broad peaks indicate small metal crystallite size, high metal dispersion and/or amorphous phase of the support. The presence of metals in the catalysts were identified with the standard JCPDS files. In all the catalysts and AC supports, peak assignments from carbon (JCPDS file no. 01-082-9929) were detected at $2\theta$=24.6° and at $2\theta$=43.7°. From the diffractogram of AC-S, a peak at $2\theta$=29.3° was detected corresponding to $CaCO_3$ (no. 04-007-8659).

Peaks of platinum were sharper than those of ruthenium and nickel. According to JCPDS file no. 00-004-0802, cubic platinum (Fm-3m) was present corresponding to peaks Pt (111) at $2\theta$=39.8°, Pt (200) at $2\theta$=46.2° and Pt (220) at $2\theta$=67.5°. In addition, peaks of $Pt_3O_4$ (no. 04-001-2426) were found from the 1.5Pt/AC-S and 3Pt/AC-S catalysts, indicating that not all platinum was present at the metallic state. For Ru catalysts, JCPDS file no. 04-001-0053 presented hexagonal ruthenium (P63/mmc) corresponding to Ru (101) at $2\theta$=43.8°. However, peaks with small intensity were difficult to detect. In the prepared nickel catalysts, the metal seemed to be present in the oxidized form of NiO (no. 01-078-4367) at $2\theta$=36.7° and at $2\theta$=62.2°. Since mainly broad peaks were detected, the calculation of metal particle size using the Scherrer equation was not made.

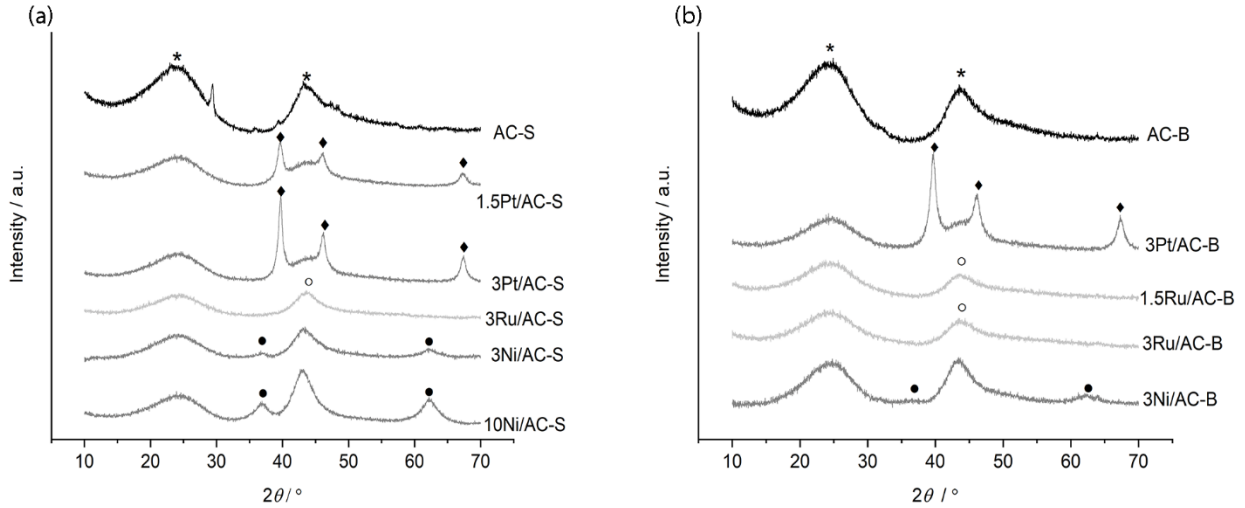


**Figure 3.** X-ray diffractograms from (a) spruce-based support and (b) birch-based support, and Pt, Ru and Ni catalysts prepared on activated carbons. Diffraction peaks are marked as follows: * = carbon at 2θ=24.6° and 2θ=43.7°, ♦ = Pt (111) at 2Θ=39.8°; Pt (200) at 2Θ=46.2°; Pt (220) at 2Θ=67.5°, ○ = Ru (101) at 2Θ=43.8°,● = NiO at 2Θ=36.7° and 2Θ=62.2°.

### *X-ray photoelectron spectroscopy*

X-ray photoelectron spectroscopy (XPS) (detection depth < 10 nm) was used to detect surface groups, especially oxygen containing groups on activated carbon supports and the impregnated catalysts. XPS was also used to detect metal oxidation states in catalysts. Analyses were performed on thermally treated, unreduced samples.

The C1s spectra of the supports and the 3Pt/AC-S catalyst are presented in the Supporting Information. From the C1s spectra, carbon containing groups could be divided into various peaks based on the binding energies (BE) (Table S1 in Supporting Information): $sp^3$ carbon-carbon bonding (BE = 284.8 eV), $sp^2$ C-C (285 eV), carbon species in alcohol or ether groups (*BE* = 286.3–287.0 eV), carbon in carbonyl groups (*BE* = 287.5–288.1 eV), carbon in carboxyl or ester groups (*BE* = 289.3–290.0 eV) and shake-up satellite due to π–π* transition in aromatic rings (*BE* = 291.2–292.1 eV). Peaks at ~285 eV can also originate from contaminates, for example Ru oxide gives a peak at 285 eV. Peaks in the region of 286.3-287.5 eV may also present structures of C–N. According to C1s scans, the surfaces of the supports consisted mostly of carbon-carbon type bonds and to some extent of functional groups, which can be acidic or basic in nature (e.g. alcohol, ether, carbonyl, quinone, carboxylic or ester type bonds). Also, minor levels of aromatic rings (from π–π* transitions) were detected. Overall, both supports had almost same characteristics according to C1s measurements.

The total oxygen from O1s scans was also calculated (Table S1 in Supporting Information), which highlighted that some metal-oxides were present. The highest amount of oxides were detected in nickel catalysts, especially in the 10 Ni/AC-S (4% of oxides), which is in line with the XRD analysis.

Figure 4 shows the x-ray photoelectron spectra of Pt4f, Ru3d and Ni2p scans. The $Pt4f_{7/2}$ signal (Fig. 4a) at 71.6 eV and $Pt4f_{5/2}$ at 74.6 eV were related to zero-valent platinum.[60] From the Pt4f XPS analysis, no oxides were detected in the platinum catalysts, while the slightly increased total oxygen content (Table S1 in Supporting Information) of the Pt/AC-S catalysts might indicate that some oxides were present. Commercial 1 wt.% Pt/AC catalyst was compared to the prepared Pt catalysts: the characters from the XPS analysis were almost identical with the 1.5Pt/AC-S catalyst.

For Ru catalysts, the Ru3d XPS peaks (Fig. 4b) were more difficult to interpret since the peaks from C1s overlapped the Ru peaks. However, peaks at 286 eV indicated the presence of metallic Ru and peaks around 284 to 285 eV the presence of $RuO_2$. Also, the increased total oxygen content from O1s scans indicated the presence of Ru oxides.[61] With XRD, no Ru oxides were detected, but it could be because of the small size of Ru crystallites.

From Ni2p scans (Fig. 4c), the main peak at ~855 eV and the broad satellite at 860 eV indicated the presence of nickel as oxide mixtures (NiO, NiOOH or $Ni(OH)_2$) in all the Ni catalysts. Metallic nickel should give a signal peak at 852.6 eV,[62] and since no peak was detected in that area, it was concluded that no metallic Ni was present in catalysts. Moreover, the increased oxygen content in the O1s scan confirmed the presence of Ni oxides in catalysts, especially in the AC-S supported Ni catalysts. These results match with XRD: metallic Pt and Ru were already present in catalysts without a reduction step but Ni was present only in oxidized forms regardless of the support.

### *Temperature programmed measurements*

The total amount of acidic surface groups was probed by temperature programmed desorption of ammonia ($NH_3$-TPD). No acidic surface groups were detected on the supports or on the noble metal catalysts (Fig. S7 and S8 in Supporting Information). However, with Ni catalysts, a small peak was obtained at 450 °C, which could be related to the presence of NiO.[63]

Temperature programmed reduction (TPR) was conducted for the supports and the 3 wt.% catalysts to reveal metal reduction temperatures (Figure 5). For both supports, a small peak was obtained at 600 °C. As Pt was added to the support, the spillover

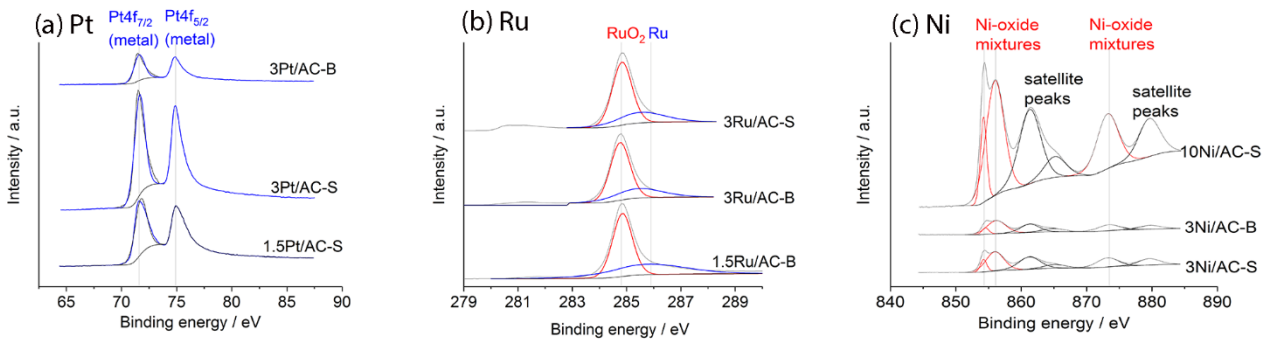


**Figure 4.** X-ray photoelectron spectra of metals on impregnated and thermally treated catalysts: (a) Pt4f region, (b) Ru3d region and (c) Ni2p region.

phenomenon occurred,[64] and wide peak from 400 to 650 °C was detected. The absence of peaks at lower temperature indicates that Pt was already in metallic form, which is in line with the XRD and XPS analysis. The Ru catalysts had small peak at around 90 °C that can be attributed to reduction of ruthenium oxide.[23] The peak around 475 °C is related to the reduction of AC surface functional groups and hydrogen spillover.[23,65]

Three different reduction temperatures were observed from the TPR profiles of the Ni catalysts. As presented in the literature, the low temperature peaks at 240 °C and 350 °C are attributed to the reduction of NiO species with little interaction with the AC.[65,66] The main peak at 475 °C is attributed to the reduction of NiO having strong interaction with the AC. Moreover, the peaks at high temperature have also been reported to occur due to hydrogen spillover and gasification of the AC support.[65,66]

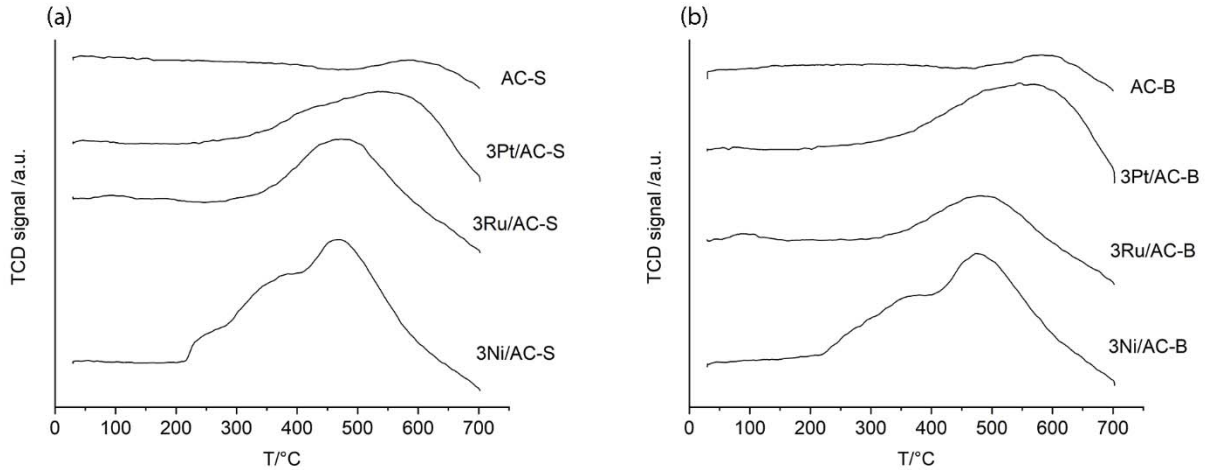


**Figure 5.** Temperature programmed reduction profiles of (a) spruce-based support and (b) birch-based support, and the 3 wt.% Pt, Ru and Ni catalysts.

## Furfural hydrotreatment

Furfural hydrotreatment experiments to produce 2-methylfuran as target compound were carried out with various metal catalysts supported on the activated carbons prepared from spruce and birch. The effect of the support, reaction temperature and metal loading were studied separately to optimize the production of the desired product. The main objective was to study the feasibility of biomass-based activated carbons as catalysts supports in MF production. However, furfural hydrotreatment reaction network (Scheme 1) is complex, and several side reactions were also observed.

### *Comparison of metals and activated carbons*

The suitability of the prepared steam-activated carbons as catalysts supports was studied at 230 °C for 300 minutes with each active metal (Ni, Ru and Pt). For each tested metal, the best support (AC-B or AC-S) in terms of producing MF was selected for further studies. Figure 6 presents the achieved MF yields as a function of contact time with the prepared catalysts having nominal 3 wt.% metal loading. It can be observed from Table 2 that the measured metal loads between the catalysts varied, which is compensated by using the contact time instead of the reaction time in Fig. 6. For Pt and Ni, the AC-S supported

catalysts produced more MF than the AC-B supported catalysts. However, in case of Ru catalysts, the catalyst supported on the AC-B produced more MF. The product distributions of all experiments conducted at 230 °C are presented in Table 5. In addition to MF, the other observed products were mainly furfuryl alcohol (FA), tetrahydrofurfuryl alcohol (THFA), 2-methyltetrahydrofuran (MTHF), furan, 2-pentanone (PN) and furanmethanol acetate (FMA). As can be noticed from Scheme 1, furfuryl alcohol is an intermediate product that will further react to MF. It indicates that potential maximum MF yields were probably not achieved with the 1.5Ru/AC-B and 3Ni/AC-B catalysts that had relatively high furfuryl alcohol yields after 300 min reaction time (Table 5). Besides the above-mentioned products, traces of similar furfural and MF dimer structures as presented by Fuente-Hernández et al.[67] were observed.

The formation of acetone was also observed. However, acetone is not formed through furfural hydrogenation but either from the dehydrogenation of the solvent (2-propanol) or the catalytic transfer hydrogenation reaction (CTH) between furfural and the solvent leading to FA and acetone.[68,69] Jaatinen and Karinen[70] studied recently the CTH properties of 2-propanol with Ni/C catalyst. It was noticed that furfural can be converted to furfuryl alcohol even without extra hydrogen via CTH with acetone as byproduct. However, the reaction was slow and almost no MF was produced. When 40 bar hydrogen gas was added at the same reaction conditions, the selectivity to MF increased.[70] Similar observation was reported by Fu et al.[71]: close to 100% selectivity to FA without extra hydrogen in 2-propanol with Ni-Cu catalyst. Chang et al.[72] also studied 2-propanol CTH properties in furfural hydrotreatment. They utilized bimetallic catalysts (Cu-Ni, Cu-Ru, and Cu-Pd) without added hydrogen and obtained FA as the main product with Cu-Ni and Cu-Ru catalysts. Interestingly, with Cu-Pd, the main product obtained was MF.

All the tested catalysts were active in furfural hydrotreatment as the conversions were over 97% (Fig. S9 in Supporting Information). However, the initial reaction rates of furfural and selectivity towards MF varied significantly. The initial reaction rates, defined here as the consumption of furfural as an average in the first 15 min reaction time per metal loading, of the Ni catalysts were low: 2.6 and 2.5 mol $g^{-1}$ wt.$\%^{-1}$ $min^{-1}$ for the 3Ni/AC-S and the 3Ni/AC-B respectively. With noble metals on AC-S, higher initial reaction rates were achieved: 8.7 and 6.5 mol $g^{-1}$ wt.$\%^{-1}$ $min^{-1}$ for the 3Pt/AC-S and the 3Ru/AC-S respectively. However, the AC-B supported noble metal catalyst had similar or only slightly higher initial reaction rates than the Ni catalysts: 2.6 and 3.8 mol $g^{-1}$ wt.$\%^{-1}$ $min^{-1}$ for the 3Pt/AC-B and the 3Ru/AC-B respectively. With all the tested catalysts, the initial furfural consumption was higher on the spruce-based supports.

With all the tested metal catalysts, a ring-opening reaction of MF to 2-pentanone (minor product) was more abundant on the spruce-based support. Zheng et al.[4] reported high yields of MF ring-opening products, especially 2-pentanone (>27%), in furfural hydrotreatment experiments conducted at 300 °C using Ni containing multicomponent catalyst (Cu/Cr/Ni/Zn/Fe). Moreover, the amount of produced 2-pentanone increased with increasing reaction temperature in the study conducted by Zheng et al.[4] Recently, Date et al.[73] investigated the effect of various supports

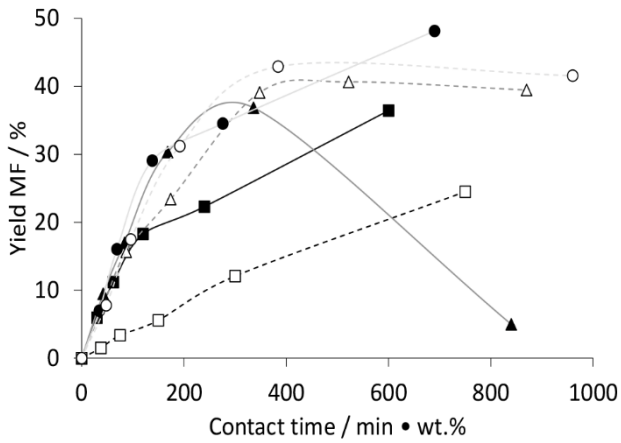


**Figure 6.** 2-Methylfuran yield as a function of contact time on various catalysts at 230 °C and 40 bar $H_2$. ● = 3Pt/AC-S, ○ = 3Pt/AC-B, ▲ = 3Ru/AC-S, Δ = 3Ru/AC-B, ■ = 3Ni/AC-S, □ = 3Ni/AC-B.

on the hydrogenation and decarbonylation of furfural with Pd. They discovered that the activated carbon support had the highest selectivity to MTHF (40%) as well as the second highest selectivity to MF (18%). Moreover with $TiO_2$ support, they achieved the highest selectivity to ring-opening products (52%) due to it's surface acidity.

In the literature, high decarbonylation activity of furfural to furan has been achieved with noble metal catalysts, especially Pd and Pt, in a gas phase system.[74,75] In our experiments, both Pt and Ru catalysts produced slightly more furan than the Ni catalysts (Table 5). Alternatively, Ni catalysts produced more THFA than the noble metal catalysts. THFA can be produced either as a hydrogenation product of furfural or furfuryl alcohol. Ni has been demonstrated in various studies to produce high yields of THFA from furfural.[76–78] Moreover, in the industrial scale, nickel catalysts are used to produce THFA.[6]

The nickel catalysts had lower metal loading than the corresponding 3 wt.% noble metal catalysts, and also the dispersion of the nickel was low. The low dispersion of especially the 3 wt.% Ni/AC-B catalysts resulted in poor performance of this catalyst. In previous studies made in our laboratory, nickel-based catalysts on commercial activated carbons have proven to be better in producing MF.[22,33] However, it was noted that 3Ni/AC-S catalyst achieved close to the same MF yield as the 3Ru/AC-S catalyst despite the low dispersion. Moreover, the spruce-based Ni catalyst seemed to be both faster at the beginning of the reaction, as well as leading to higher final MF yield than the AC-B supported nickel catalyst. However, in case of the birch-based support, significant amount of furfuryl alcohol was still present after 300 min reaction time (Table 5) indicating that the MF yield could be higher with a prolonged reaction time. The lower activity of the AC-B supported nickel might be explained by the slightly lower dispersion of the 3Ni/AC-B compared to the 3Ni/AC-S. Low dispersion of Ni on AC-B might be explained by the calcium aggregates, which were present according to the EDS.

The two supported Ru catalysts performed differently in the hydrotreatment experiments conducted at 230 °C (Fig. 6). Typically after reaching the highest observed MF yield, the desired product started to slowly hydrogenate further as observed

**Table 5.** Furfural conversion at highest observed MF yield, corresponding reaction time and product yields at 230 °C and 40 bar $H_2$.

| Catalyst | $X$ /% | $t$ /min | $Y_{MF}$ /% | $Y_{FA}$ /% | $Y_{THFA}$ /% | $Y_{MTHF}$ /% | $Y_{Furan}$ /% | $Y_{FMA}$ /% | $Y_{PN}$ /% |
|---|---|---|---|---|---|---|---|---|---|
| 1.5Pt/AC-S | 99.4 | 300 | 47.3 | 5.7 | 0.9 | 0.0 | 2.1 | 0.4 | 0.3 |
| 3Pt/AC-S | 99.8 | 300 | 48.2 | 3.8 | 1.1 | 0.0 | 2.5 | 0.0 | 0.5 |
| 3Pt/AC-B | 98.1 | 120 | 43.0 | 6.3 | 0.8 | 0.0 | 5.4 | 1.7 | 0.1 |
| 1.5Ru/AC-B | 99.3 | 300 | 34.7 | 17.4 | 1.8 | 0.0 | 3.5 | 2.0 | 0.0 |
| 3Ru/AC-S | 99.0 | 120 | 36.9 | 9.3 | 2.7 | 0.9 | 2.7 | 0.7 | 0.8 |
| 3Ru/AC-B | 99.5 | 180 | 40.7 | 2.4 | 1.5 | 0.0 | 2.8 | 0.7 | 0.2 |
| 3Ni/AC-S | 97.3 | 300 | 36.4 | 2.5 | 3.7 | 0.0 | 2.2 | 0.8 | 0.1 |
| 3Ni/AC-B | 99.0 | 300 | 24.5 | 21.7 | 5.7 | 0.6 | 2.0 | 0.7 | 0.0 |
| 10Ni/AC-S | 99.6 | 300 | 37.0 | 9.1 | 6.2 | 1.6 | 1.5 | 0.1 | 0.5 |

from Figure 6, where the MF yields are quite stable after reaching the maximum (3Ru/AC-B and 3Pt/AC-S). The further reaction of MF was fast with the 3Ru/AC-S catalyst compared to the other catalysts. The maximum obtained MF yield with the 3Ru/AC-S catalyst was about 37% after 120 min reaction time, which was somewhat lower than what was reached with the 3Ru/AC-B catalyst (41% after 180 min). By observing Fig. 6, it seems that the maximum MF yield for the 3Ru/AC-S catalyst could have been between the sampling times as samples were not taken between the reaction times of 60 and 120 min or between 120 and 300 min. The fast hydrogenation of MF in this experiment was confirmed by repeating the experiment. MF reacted to MTHF, 2-pentanone, alcohols (including mainly 2-pentanol but also pentanediols) and condensation products. The hydrogenation of MF might be due to CTH reaction as significantly higher concentration of acetone was obtained with the 3Ru/AC-S catalyst compared to other catalysts. Furfural CTH reaction in 2-propanol with commercial 5 wt.% Ru/C was studied by Panagiotopoulou et al.[23,79] They obtained 51% MF yield, and the authors also discovered that the active phase of catalyst involved both metallic and oxidized Ru. The dispersion of the Ru supported on AC-B was a bit higher and the particle size slightly smaller compared to the AC-S supported catalyst. There were also differences in the XPS analysis of the Ru catalysts as the 3Ru/AC-B contained significantly more oxygen that the spruce-based catalyst. However, the in-situ reduction prior to the experiments was likely to compensate the difference, and the reason for the possible CTH activity of the 3Ru/AC-S catalyst remained unclear.

Both Pt catalysts performed in a relatively similar manner during the experiments at 230 °C (Fig. 6). However, the highest observed MF yield was achieved earlier with the catalyst having birch-based support (Table 5). This was surprising since with Ru, the AC-S supported catalysts achieved the highest observed MF yield faster than the AC-B supported catalyst. Moreover, it can be noticed that with the AC-B supported Pt catalyst, the amount of produced furan after 120 min reaction time was more than double compared to the amount of furan produced after 300 min reaction time with the spruce-based Pt catalysts. Similarly, Ru catalysts supported on AC-B produced more furan than the 3Ru/AC-S (Table 5). This indicates that the decarbonylation of furfural might be promoted with noble metals supported on AC-B. Moreover, the AC-B supported Pt catalyst produced 1.7% FMA whereas with the AC-S support, no FMA was produced. The formation of this relatively large condensation product was noticed to be favored by large pores by Jaatinen et al.[80] The 3Pt/AC-B catalyst had more mesopores than the 3Pt/AC-S catalyst (Table 4) which could explain the formation of FMA; however, no similar behavior was observed with Ru or Ni. The highest obtained MF yield from all the experiments conducted at 230 °C was achieved with the Pt/AC-S catalyst (48%) that had the highest metal dispersion (37%) and the smallest particle size (2.7 nm).

### *The effect of reaction temperature*

The effect of reaction temperature was investigated at 210 °C, 230 °C and 240°C (Figure 7). Other authors have reported higher MF yield when increasing reaction temperature and/or time over Ru/C catalyst.[23] However, it has been reported elsewhere that furfuryl alcohol undergoes a highly exothermic polymerization reaction when heated up to 250 °C.[81] Thus temperatures over 240 °C were not tested. Moreover, based on our earlier studies, temperatures below 200 °C were not found effective for MF production.[22] Figure 7 presents the MF yield as a function of contact time for Pt, Ru and Ni catalysts at the studied temperatures. The $H_2$ pressure was 40 bar in all the experiments, and the AC support was originating from spruce for Ni and Pt and from birch for Ru. The selection of the support for each metal was based on the higher achieved MF yields in experiments conducted at 230 °C.

The effect of the reaction temperature on the obtained MF yield was the least with nickel catalysts. The highest MF yield (36%) was almost the same in all tested temperatures, but the potential maximum yield was not reached at all of the studied temperatures since significant amounts of FA were detected from

the final samples (FA yields of 22% and 7% at 210 °C and 240 °C respectively). It means that longer reaction time is needed to reach the potential maximum MF yield. However, at 230 °C, most of the furfuryl alcohol had already reacted further (FA yield of 2.5%) to MF and other products, such as THFA, furan and FMA, indicating that the MF yield was already close to the maximum value. Moreover, the conversions were over 96%.

Higher temperature resulted in higher obtained MF yields with shorter reaction times in the case of both noble metal catalysts. The maximum obtained yields were 49% and 50% for 3Ru/AC-B and 3Pt/AC-S at 240 °C respectively, and they were reached after 120 min reaction time. Moreover, the increase of the temperature by just 10 °C (from 230 °C to 240 °C) had a much more significant effect on the yield than the change from 210 °C to 230 °C. At 240°C, the produced MF started to hydrogenate further, which can be seen as a drop in the MF yield after the maximum was reached (Fig. 7). In the literature, 40% MF yield was achieved in liquid phase at 175 °C (30 min) using a commercial 5 wt.% Pt/C catalyst[26]. With commercial 5 wt.% Ru/C catalysts, MF yield of 51% at 180 °C[23] and selectivity of 18.9% at 165 °C[27] were reported in liquid phase batch systems. As a comparison, better MF yield was obtained with our Pt catalyst and similar MF yield with our Ru catalyst on biobased activated carbon.

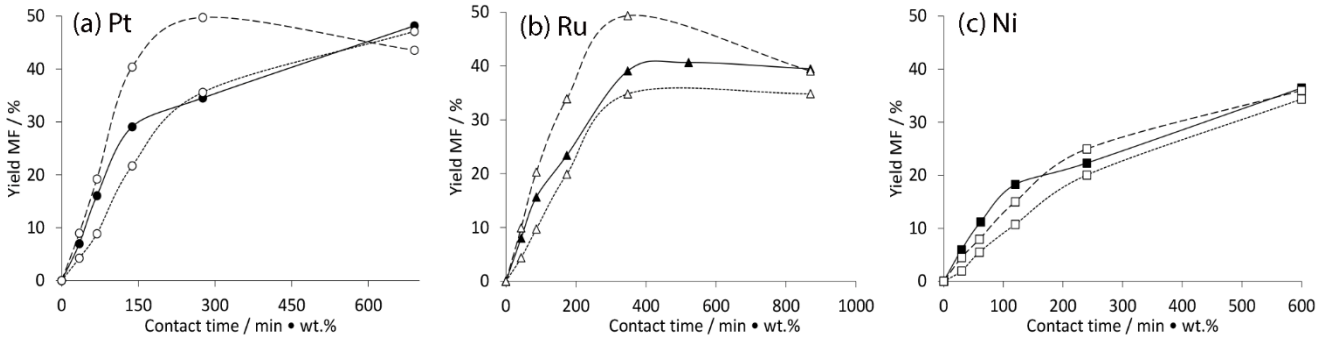


**Figure 7.** 2-Methylfuran yield as a function of contact time in various temperatures. (a) 3Pt/AC-S; ● = 230 °C, ○ (dashed) = 240 °C, ○ (dotted) = 210 °C, (b) 3Ru/AC-B; ▲ = 230 °C, Δ (dashed) = 240°C, Δ (dotted) = 210°C, (c) 3Ni/AC-S; ■ = 230 °C, □ (dashed) = 240 °C, □ (dotted) = 210 °C.

### *The effect of metal loading*

The effect of the metal loading was investigated at 230 °C. Figure 8 presents the MF yield as a function of contact time in experiments with 1.5 and 3 wt.% Pt/AC-S, 1.5 and 3 wt.% Ru/AC-B and 3 and 10 wt.% Ni/AC-S. In addition to the reaction rate, also the yield of produced MF differs with various metal loadings. As previously mentioned, the supported nickel catalysts were not as effective as noble metal catalysts in producing MF. The 10Ni/AC-S was observed to be slower in MF production as a function of contact time in the beginning of the reaction compared to the 3 wt.% Ni catalyst. However, after 300 min reaction time, both catalysts achieved similar MF yield of ca. 37%. This rather surprising effect might be explained by metal particle size and dispersion. The dispersion was significantly lower and the particle size higher with the 10 wt.% catalyst. Ni catalyst deactivation, which is further discussed later, could also affect the performance of these catalysts.

The catalyst with lower Ru loading (1.5Ru/AC- B) was slower in producing MF than the 3 wt.% Ru catalyst as a function of contact time. Moreover, the 3 wt.% catalyst achieved the highest observed MF yield of 41% after 180 min reaction time, but the 1.5 wt.% catalysts did not reach the potential maximum yield even after 300 min. The lower activity towards MF was also indicated with a significant amount of furfuryl alcohol (yield 17%) in the final product mixture. It is likely that longer reaction time would have led to higher final MF yield. However, it would probably not be significantly higher than with the 3 wt.% catalyst. The dispersion and metal particle size had a correlation with the reaction rate as the 1.5 wt.% Ru catalyst had lower dispersion and larger particle size which was observed to make the catalyst less effective in producing MF.

With both Pt catalysts, the production rate of MF was similar in the beginning of the reaction. The 1.5 wt.% Pt/AC-S also achieved similar final MF yield as the corresponding 3 wt.% catalyst. This is remarkable since the spot price of an ounce of Pt is around 930 USD.[82] Moreover, the overall product distributions were also similar. The dispersion of the 1.5 wt.% Pt catalyst was only slightly lower than with the 3 wt.% Pt catalyst and was considered high compared to other prepared catalysts. Moreover, the surface area was slightly higher with the lower Pt loading. Based on XPS C1s analysis, the two catalysts appeared to be similar.

### *Analysis of the gas phase*

Qualitative gas phase analysis confirmed that the product gases contained mainly hydrogen as a left over from the experiments. Gaseous reaction products included small amounts methane, ethane, carbon dioxide, carbon monoxide and some heavier hydrocarbons. Out of these gases, methane, ethane and carbon dioxide were the most abundant. When comparing the peak areas of gaseous products from the experiments conducted at 230 °C (3 wt.% catalysts), the spruce-based support favored the production of gaseous hydrocarbons compared to birch-based support. Moreover, the production of methane and ethane was higher with the spruce-based support with the noble metals, but with Ni, no difference was detected. Among the noble metals,

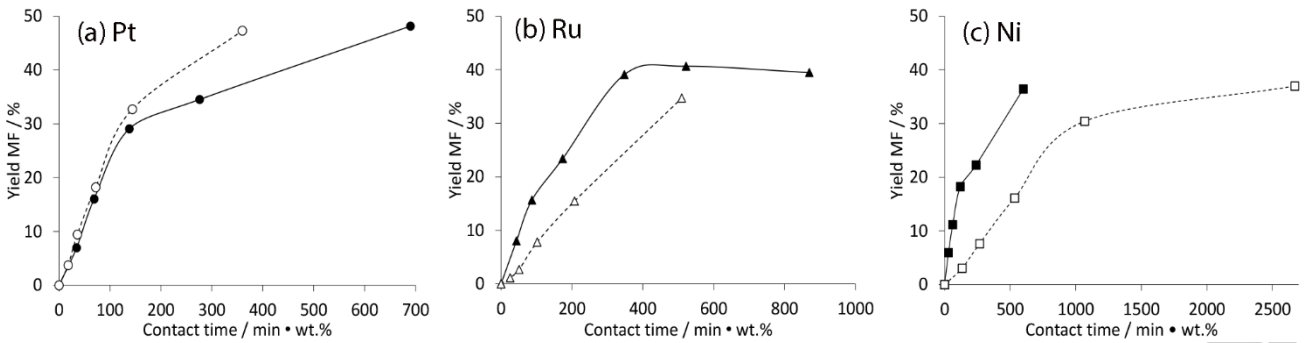


**Figure 8.** 2-Methylfuran yield as a function of contact time with various metal loading. (a) ○ = 1.5Pt/AC-S, ● = 3Pt/AC-S, (b) Δ = 1.5Ru/AC-B, ▲ = 3Ru/AC-B, (c) ■ = 3Ni/AC-S, □ = 10Ni/AC-S. $T$ = 230 °C, $p$ = 40 bar $H_2$.

gaseous products were produced more with Ru.

The reaction temperature also affected the formation of gaseous products. The highest amount of hydrocarbons was produced at 240 °C with all the catalysts. Moreover, the 1.5 wt.% noble metal catalysts produced less gaseous products than the corresponding 3 wt.% catalysts, and the 10 wt.% Ni catalyst more than the corresponding 3 wt.% catalyst.

### *Conclusions of the hydrotreatment experiments*

Based on all the experiments, noble metal catalysts were superior in the production of MF compared to nickel catalysts when wood-based activated carbon supports were utilized. Compared to our previous studies made in our laboratory,[33] the prepared nickel catalysts on birch- and spruce-derived AC were not as effective in producing MF as impregnated Ni catalysts on commercial activated carbon supports. Based on the TPR measurements, the in situ reduction temperature (250 °C) was insufficient for nickel, which could be one explanation for the lower performance of the Ni catalysts. However, the reduction temperature was limited by the capacity of the reactor oven, and higher temperatures were not possible in our study. Based on the TPR analysis, Ru and Pt were likely to be present at metallic state after reduction, but Ni was not. That means the noble metals were more easily reduced. However, also the oxidized metals have been noticed to take part in furfural hydrogenolysis, and the combination of reduced and oxidized metal improves MF yields at least with Ru.[23] This could overcome the challenge related to the too low reduction temperature at least to some extent. Moreover, low metal dispersions and large particles were calculated from chemisorption analysis for the Ni catalysts that were unfavorable characteristics in MF production.

The noble metal catalysts performed well compared to other studies conducted in liquid phase[6] since only 1.5 and 3 wt.% loadings achieved MF yields of 47-49%. However, even better results have recently been reported with bimetallic catalysts. For example Srivastava et al.[83] reported furfural hydrotreatment study in liquid phase using Cu-Co catalyst on alumina and achieved MF yield of over 80%. Fu et al.[71,84] studied MF production with Ni-Cu catalyst on activated carbon and alumina, and their highest yield was 91% on activated carbon. Chang et al.[72] also studied furfural hydrotreatment and utilized bimetallic catalysts (Cu-Ni, Cu-Ru, and Cu-Pd) on $ZrO_2$ without added hydrogen, and the best obtained MF yield of 62% was achieved with the Cu-Pd catalyst.

### Characterization of spent catalysts

Selected catalysts (3Pt/AC-S, 3Ru/AC-B and 3Ni/AC-S) used in the hydrotreatment reaction at 230 ˚C were characterized with ICP analysis (Table 2), nitrogen physisorption (Table 4), TEM (Fig. 9) and XRD (Fig. 10) after usage. No other pretreatment except washing with water and drying was performed when the catalysts were taken from the catalyst basket.

ICP analysis for spent catalysts were performed to verify the metal amount after testing. The results showed (Table 2) that the metal content of Ru catalyst was decreased significantly during the reaction indicating the leaching of the metal. However, Pt and Ni contents were close to the values of fresh catalysts after reaction (decrease of 0.2–0.3 wt.%).

The pore volume of the Pt catalyst decreased circa 25% during the reaction, but mainly micropores were lost while mesopores remained available. This indicates that the catalyst was not fully deactivated. The pore volume of the Ru catalyst decreased circa 59% during the reaction and even 40% of the mesopores were lost. With the Ni catalyst, most of the pores were lost (95% of micropores and 58% of mesopores) during the experiment. The pore volume decrease might be because of the partial collapse of the bulk material, the agglomeration of metal particles due the high pressure or the formation of coke in the pores. The significant pore blocking of the Ni catalyst could explain why the higher reaction temperature did not result in higher MF yields assuming that the pore blocking happens fast after starting the reaction.

TEM images (Fig. 9) of spent catalysts showed that the particle sizes of Pt and Ru were 3-5 nm and 1-3 nm respectively, which were almost the same as in fresh catalysts. This indicates that no significant sintering of noble metals was detected. Ni particles had a size of 5-10 nm which was similar to the fresh catalyst; nevertheless, also bigger aggregates, over 20 nm, were found. In this case, some sintering or agglomeration happened

with nickel metal particles, which could explain the decreased surface area and pore volume.

XRD diffractograms with standard JCPDS files confirmed the presence of metals in the used catalysts (Fig. 10). Cubic platinum (Fm-3m) was present corresponding to peaks Pt (111) at 2$\theta$=39.8°; Pt (200) at 2$\theta$=46.2° and Pt (220) at 2$\theta$=67.5° in the 3Pt/AC-S catalyst. For 3Ru/AC-B, hexagonal ruthenium (P63/mmc) was detected corresponding to Ru (101) peak at 2$\theta$=43.8°; however, the peak with small intensity was difficult to detect. For 3Ni/AC-S catalyst, cubic nickel (Fm-3m) was present corresponding to peaks Ni (111) at 2$\theta$=44.4° and Ni (200) at 2$\theta$=51.8°. Moreover, cubic NiO (Fm-3m) was detected from the sample corresponding to peaks at 2$\theta$=37.3° and 2$\theta$=63.9°. Based on the XRD analysis of the used catalyst, the noble metals were fully reduced and remained at metallic state after testing in reaction. Instead, nickel was still partly oxidized which was expected, as the reduction temperature (250 °C) was not enough to reduce nickel oxides to metallic. Another reason could be the oxidizing of Ni after taking the catalyst from the reactor.

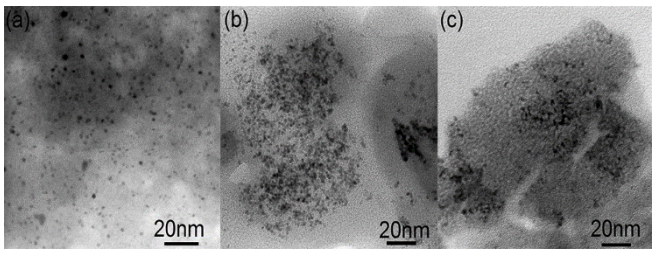


**Figure 9.** Bright field TEM images from used catalysts: (a) 3Pt/AC-S, (b) 3Ru/AC-B, (c) 3Ni/AC-S.

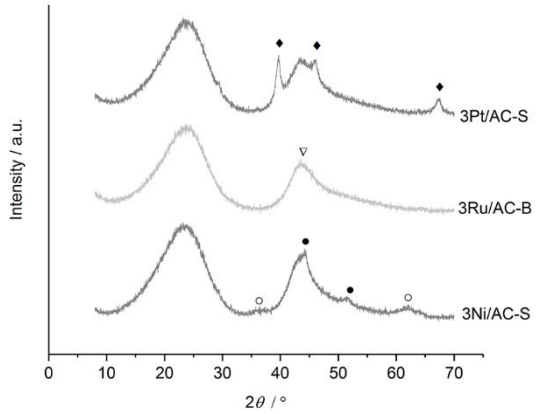


**Figure 10.** X-ray diffractograms of the spent 3 wt.% catalysts. Diffraction peaks are marked as follows: ♦ = Pt (111) at 2Θ=39.8°; Pt (200) at 2Θ=46.2°; Pt (220) at 2Θ=67.5°, ∇ = Ru (101) at 2Θ=43.8°,● = Ni (111) at 2Θ=44.4°; Ni (200) at 2Θ=51.8°, ○ = NiO at 2Θ=37.3° and 2Θ=63.9°.

## Conclusions

Biobased carbon supports from lignocellulosic biomass (spruce and birch) were prepared by carbonization and steam activation. These activated carbons were used as supports for noble metals (Pt, Ru) and lower-cost nickel catalysts. The catalysts were tested in a batch reactor for furfural hydrotreatment to produce a potential biofuel component, 2-methylfuran.

Both activated carbons were suitable catalyst supports for furfural hydrotreatment, and the prepared catalysts were active reaching close to 100% furfural conversion and high yields to MF. The initial reaction rates observed for AC-S supported catalysts were higher than for AC-B supported catalysts. Despite the small differences in the bulk material, such as residual metals and oxygen content, neither of the supports was found to be superior to each other. The most important factors for the catalyst's ability to produce MF were found to be the metal dispersion and particle size regardless of the support.

Another factor affecting the MF production was the reaction temperature. In this work, tests were carried out at 210-240 °C. The two noble metal catalysts (Pt and Ru) produced the highest observed MF yields (50% for 3Pt/AC-S and 49% for 3Ru/AC-B) at the highest tested temperature (240 °C). The highest observed yields were reached after a relatively short reaction time of 120 min. With both noble metal catalysts, continuing the reaction at 240 °C led to further hydrogenation products causing the MF yield to decrease after the observed maximum. Moreover, the performance of the noble metal catalysts was better compared to the nickel catalysts with the highest observed MF yield of 37% (10Ni/AC-S at 230 °C). Unlike the noble metal catalysts, the reaction temperature did not have such an effect on nickel catalysts. The severe loss of surface area during the reaction is likely to have caused the relatively similar performance of the nickel catalyst at all tested temperatures.

The metal loading also affected the experimental results. However, the effect was more likely caused by the difference in dispersion and particle size among the catalysts and not exactly due to the metal load. The 1.5 wt.% Pt catalyst was found to have high dispersion and a similar surface structure as the 3 wt.% Pt/AC-S which might explain the preferable performance of the catalyst. Moreover, the lower Pt loading was found to be almost as effective as the 3 wt.% catalyst in producing 2-methylfuran. The low metal loading can enable the production of MF with high yields and reduced catalyst costs.

## Experimental Section

### Materials

Lignocellulosic forest-residue-based birch and spruce from Finland were utilized as carbon sources. Catalytic precursor materials were $Ni(NO_3)_2$ 6 $H_2O$ (Ni 99.0-102.0% w/w) purchased from ACS, $Pt(NO_3)_4$ (Pt 15% w/w) and $Ru(NO)(NO_3)_3$ (Ru 31.3% w/w) purchased from Alfa Aesar. One commercial 1% platinum on activated carbon catalyst was obtained from Degussa (Type F 103 R).

All chemicals used in the catalyst performance tests or in calibrations were purchased from Sigma-Aldrich. Furfuryl alcohol (98%), furan (≥99%), 2-methylfuran (99%), tetrahydrofurfuryl alcohol (99%), 2-methyltetrahydrofuran (anhydrous, ≥99%), 2-propanol (≥99.5%), 2-butanol (99%), 2-pentanol (98%), cyclopentanol (99%), 2-pentanone (99.5%) and cyclopentanone (≥99%) were utilized without purification. Furfural (99%) was purified with distillation into a final molar purity of 99.8%.

**Activated carbon support and catalyst preparation**

The biomass (birch and spruce) was dried, carbonized and steam-activated in a one-step process in a rotating quartz reactor (Nabertherm GmbH RSRB 80). The thermal profile during the whole process was divided into two parts. The first carbonization step, in which the temperature was raised to 800 °C with a ramp of 6.7 °C /min, procured the total carbonization of the biomass followed by the activation step. During the activation, the temperature was kept at 800 °C for 120 min with a stream of water steam (120 g $h^{-1}$ at 140 °C) creating the proper surface activation. During the whole process, the reactor was flushed with an inert gas. In the ramping step only $N_2$ (flow 200 ml $min^{-1}$), and in the activation step both carrier gas ($N_2$ flow 200 ml $min^{-1}$) and steam (120 g $h^{-1}$ at 140 °C) were utilized. The resulting activated carbon was crushed and sieved to fraction size of 1.4-2 mm.

The crushed AC was dried overnight at 105 °C without any further pretreatment. Catalysts containing nominal 1.5, 3 or 10 wt.% of metal were prepared by incipient wetness impregnation of the metal nitrates as a precursor. Metal precursors of nickel, platinum and ruthenium were added to the AC and rotated overnight in a rotating mixer (Rotavapor). After impregnation at room temperature, the catalysts were dried overnight at 105 °C. The thermal treatment step was performed in a chemical vapor deposition (CVD) oven at 350 °C for 5 hours and flushed with nitrogen (240 ml $h^{-1}$ $g_{cat}^{-1}$) during the whole process.

**Catalyst characterization**

The percentage of total carbon present in the prepared ACs was measured using a Skalar Primacs MCS instrument. Dried samples were weighted in quartz crucibles, combusted at 1100 °C in a pure oxygen atmosphere, and the formed $CO_2$ was analyzed by an infrared (IR) analyzer. The total mass of carbon in each sample was calculated as a percent of the mass initially weighted. Ash content was determined by using SFS-EN 14775 standard method.[85]

Elemental analysis was performed using a Flash 2000 CHNS-O Organic elemental analyzer by Thermo Scientific. The ground and dried sample (about 1 mg) was placed in the analyzer and mixed with 10 mg of vanadium pentoxide ($V_2O_5$) to enhance the burning. The prepared sample was combusted at 960 °C for 600 s using methionine as a standard for the elements: C, H, N and S, while the standard used for oxygen was 2,5-(*Bis*(5-*tert*-butyl-2-benzo-axazol-2-yl)thiophene (BBOT). Plain tin cups were used as bypass (3 pcs) when starting the measurements.

Metal contents of prepared AC and impregnated catalysts were measured by ICP-OES using a Perkin Elmer Optima 5300 DV instrument. Samples of 0.10-0.12 g were added in the mixture of 37% hydrochloric acid and 63% nitric acid and digested in a microwave oven (MARS, CEM Corporation) at 200 °C for 10 min. After digestion, the solution was diluted to 50 ml and the dissolved metals were analyzed by ICP-OES.

Point of zero charge (PZC) for the activated carbons was determined according to the batch equilibrium method.[86] Solutions of various initial pH values (2-12) were prepared by adding KOH or $HNO_3$ solutions (0.01 or 0.1 mol $l^{-1}$) to 40 ml of 0.1 mol $l^{-1}$ $KNO_3$ solution. The AC samples (0.2 g) were added into a 250 ml Erlenmeyer flask with the initial pH solutions. The mixtures were agitated for 72 hours at room temperature after which the pH was measured. The amount of $H^+$ or $OH^-$ ions adsorbed by ACs were calculated from the difference between the initial and the final concentration of $H^+$ or $OH^-$ ions.

The adsorptive properties of the activated carbons were tested by investigating the adsorption of the dyes methylene blue (MB) and orange II (OR) into the pores by the method described in the literature.[87–89] A solution containing 300 mg of MB or OR per liter of $H_2O$ was prepared, and 50 ml of this solution was transferred into a 250 ml Erlenmeyer flask. 50 mg of activated carbon was added, and the solutions were continuously agitated for 24 hours in order to achieve equilibrium between the adsorption and desorption of the tested dye. Portions of each solution were filtered and, if needed, diluted. The absorbance of the solutions were measured at 664 nm for MB and at 485 nm for OR on a Shimadzu UV-Vis 1800 double-beam spectrophotometer. The concentration of each solution was calculated from a calibration line obtained from known concentrations of MB. The absorbed mass was calculated using Equation **(1)**, and the percent of MB removed ($q$) was calculated using Equation **(2)**.

$$q(\mathrm{ads}) = (C_0 - C_t) \cdot V/m \quad \textbf{(1)}$$

$$\%\ \mathrm{removed} = (C_0 - C_t)/C_0 \quad \textbf{(2)}$$

where $C_0$ is the initial concentration of the dye (300 mg $l^{-1}$), $C_t$ is a measured concentration of the dye after 24 h, $V$ is the volume of the dye solution and $m$ is the mass of the activated carbon.

A field emission scanning electron microscope of Zeiss Ultra Plus equipped with an energy-dispersive X-ray spectroscopy (EDS) analysis system was used to study the microstructure of the catalysts and for elemental analysis.

The morphology of the catalyst particles was studied using an energy filtered transmission electron microscope (EFTEM) LEO 912 OMEGA. The catalyst samples were dispersed in acetone and pretreated in an ultrasonic bath for several minutes to create a microemulsion. A small drop of the microemulsion was deposited on a copper grid pre-coated with carbon and evaporated in air at room temperature. The metal particle sizes were estimated from TEM images of each sample. The accelerating voltage and emission current in the measurements were 120 kV and 8-15 μA respectively, while the resolution of the instrument was 0.37 nm.

Specific surface areas were calculated from adsorption isotherms of $N_2$ at isothermal conditions in liquid nitrogen according to the BET (Brunauer–Emmett–Teller) theory.[51] Pore distribution was calculated from the adsorption isotherms using the DFT (Density Functional Theory) model.[52,53] The fresh or spent catalyst samples (about 100 mg) were weighted in a quartz tube. Samples were evacuated and heated to 140 °C in order to remove any adsorbed components and moisture. The measurements were performed by a Micromeritics ASAP 2020 equipment.

Available metal surface areas were calculated from thermally treated, reduced samples by chemisorption of hydrogen or carbon monoxide using a Micromeritics ASAP 2020 or a Thermo Fisher Scientific Surfer Ultra Plus equipment. Each sample (about 500 mg) was weighted in a U-shaped quartz tube, and the sample was supported with quartz glass wool. Prior to measurements, samples were reduced in hydrogen flow under elevated temperatures (250 °C for Pt and 350 °C for Ni and Ru) after which degassing down to $10^{-5}$ Torr was performed at the same temperature for 2 h. Chemisorption measurements were performed at 35 °C for Pt and Ni and at 75 °C for Ru[57]. Dispersion and particle size were calculated as described elsewhere.[90]

X-ray diffractograms were recorded by a PANalytical X´Pert Pro X-ray diffraction equipment using monochromatic CuKα1 radiation ($\lambda$=1.5406 Å) at 45 kV and 40 mA. Diffractograms were collected in the 2θ range of 5-80° at 0.017° intervals and with a scan step time of 110 s. The crystalline phases and structures were analyzed by HighScore Plus program.

X-ray photoelectron spectroscopy analyses were performed using a Thermo Fisher Scientific ESCALAB 250Xi XPS System. The catalyst samples were placed on an indium film. With pass energy of 20 eV and the spot size of 900 μm, the accuracy of the reported binding energies were ±0.2 eV. The Ni, Pt or Ru and O, C and N were measured for all samples. The measurement data was analyzed by Avantage V5. The monochromatic AlKα radiation (1486.7 eV) operated at 20 mA and 15 kV. Charge compensation was used to determine the presented spectra, and the calibration of the binding energies (BE) was performed by applying the C1s line at 284.8 eV as a reference.

Temperature programmed desorption of $NH_3$ was performed by an AutoChem II 2920 system. Prior to the $NH_3$-TPD analysis, the samples (about 50 mg) were pre-treated in He flow of 50 ml/min at 500°C for 30 min. After that, the samples were cooled to 100 °C, and the adsorption of

ammonia (50 ml/min of 15% $NH_3$/He at 100°C) was continued for 60 min. Prior to the desorption, the samples were flushed in He flow of 50 ml/min for 30 min in order to remove all reversibly adsorbed $NH_3$. The $NH_3$ desorption was carried out from 100 to 550 °C. During the analysis, a temperature ramp of 10 °C/min and He flow rate of 50 ml/min were used.

Temperature programmed reduction (TPR) was conducted with an Altamira AMI-200 equipment connected to a thermal conductivity detector (TCD). The samples (about 10 mg) were placed in a flow-through quartz glass tube. Prior to the measurements, the samples were dried under He flow of 40 ml/min at 350 °C for 1 h after which they were cooled down to 30 °C. A cold trap between the sample tube and the detector was filled with $CO_2$ ice to prevent any leftover moisture entering the detector. A temperature ramp of 5 °C/min to 700 °C was utilized for the TPR measurements with 2% $H_2$/Ar flow of 40 ml/min.

#### Catalyst performance tests

Hydrotreatment experiments of furfural were performed in a 50 ml batch reactor from Parker Autoclave Engineers. The solvent was selected to be 2-propanol in order to promote hydrogenolysis and to avoid furan ring rearrangement.[25] In each experiment, 1 ml of furfural was mixed with 15 ml of solvent and added to the reactor from a pressurized feed tank (40 bar $H_2$). Prior to adding the feed, 0.2 g of catalyst was put into a Robinson Mahoney type catalyst basket and reduced in situ (250 °C, 2h, 40 bar $H_2$). The reactor was also heated to the desired reaction temperature before adding the feed. Stirring speed of 700 rpm was utilized in all experiments.

Samples were taken during the experiments after 0, 15, 30, 120 and 300 min of reaction and optionally other times. The liquid samples were analyzed with an Agilent 6890 Series gas chromatograph (GC) including a flame ionization detector (FID) and utilizing a Zebron ZB-wax Plus column (60 m x 0.25 mm x 0.25 µm). The GC temperature program started at 40 °C after the injection at 230 °C. Heating rate was 5 °C $min^{-1}$ until 100 °C and 20 °C $min^{-1}$ to the final temperature of 230 °C. Injection volume was 1 µl, and the internal standard was 2-butanol. Product compounds were identified using an Agilent GC-MS (7890-5975) with a similar column and temperature program. Mass spectra were collected with an electron impact ionization of 70 eV.

Furfural conversion ($X$) was calculated with Equation **(3)**, product selectivity ($S$) with Equation **(4)** and product yield ($Y$) with Equation **(5)**.

$$X = \frac{C_{\mathrm{F},0} - C_{\mathrm{F},t}}{C_{\mathrm{F},0}} \quad \textbf{(3)}$$

$$S_i = \frac{C_{i,t}}{C_{\mathrm{F},0} - C_{\mathrm{F},t}} \quad \textbf{(4)}$$

$$Y_i = \frac{C_{i,t}}{C_{\mathrm{F},0}} \quad \textbf{(5)}$$

where $C_{\mathrm{F},0}$ is furfural concentration in the feed, $C_{\mathrm{F},t}$ is furfural concentration at reaction time $t$ and $C_{i,t}$ is the concentration of a product $i$ at reaction time $t$.

The product gases were analyzed after each experiment. The reactor was first cooled to room temperature after which the sample was taken into a previously evacuated container. The gas sample was analyzed by an Agilent 6890 Series GC with a FID and a thermal conductivity detector (TDC). CO, $CO_2$, $H_2$ and $N_2$ were analyzed with the TCD connected to two columns: a HP-PLOT/Q (30 m x 0.53 mm x 40 µm) and a HP Molesieve (30 m x 0.53 mm x 25 µm). Produced hydrocarbons were analyzed with the FID utilizing a HP-AL/KCL column (50 m x 0.32 m x 8 µm). Heating program started from 40 °C with a 9.5 min hold, and the inlet temperature was 200 °C. After the hold, the heating rate was 10 °C $min^{-1}$ until the final temperature of 200 °C without any extra holds.

## Acknowledgements

Authors E. Mäkelä and S. Jaatinen acknowledge KAUTE foundation for financial support for this research paper. Author R. Lahti acknowledges the EU/European Regional Development Fund, Leverage from the EU program (within project no. A71029) for financial support. Authors would like to thank M.Sc Davide Bergna for preparing the activated carbons and Dr. Zouhair El Assal for conducting the TPD measurements. Center of Microscopy and Nanotechnology in University of Oulu (Finland) is acknowledged for FESEM and XPS analysis. Aalto University BioEconomy infra is also acknowledged for equipment support.

**Keywords:** Furfural • 2-Methylfuran • Activated carbon • Biomass • Biofuel

[1] B. Chen, F. Li, Z. Huang, G. Yuan, *Appl. Catal. A Gen.* **2015**, *500*, 23–29.

[2] S. N. Naik, V. V. Goud, P. K. Rout, A. K. Dalai, *Renew. Sustain. Energy Rev.* **2010**, *14*, 578–597.

[3] H. Zabed, J. N. Sahu, A. N. Boyce, G. Faruq, *Renew. Sustain. Energy Rev.* **2016**, *66*, 751–774.

[4] H. Y. Zheng, Y. L. Zhu, B. T. Teng, Z. Q. Bai, C. H. Zhang, H. W. Xiang, Y. W. Li, *J. Mol. Catal. A Chem.* **2006**, *246*, 18–23.

[5] X. Yang, X. Xiang, H. Chen, H. Zheng, Y.-W. Li, Y. Zhu, *ChemCatChem* **2017**, *9*, 3023–3030.

[6] K. Yan, G. Wu, T. Lafleur, C. Jarvis, *Renew. Sustain. Energy Rev.* **2014**, *38*, 663–676.

[7] H. Wei, D. Gao, L. Zhou, D. Feng, C. Chen, Z. Pei, *Fuel* **2016**, *164*, 245–253.

[8] S. Sitthisa, W. An, D. E. Resasco, *J. Catal.* **2011**, *284*, 90–101.

[9] M. Thewes, M. Muether, S. Pischinger, M. Budde, A. Brunn, A. Sehr, P. Adomeit, J. Klankermayer, *Energy and Fuels* **2011**, *25*, 5549–5561.

[10] C. Wang, H. Xu, R. Daniel, A. Ghafourian, J. M. Herreros, S. Shuai, X. Ma, *Fuel* **2013**, *103*, 200–211.

[11] H. Wei, D. Feng, G. Shu, M. Pan, Y. Guo, D. Gao, W. Li, *Appl. Energy* **2014**, *132*, 317–324.

[12] H. Xiao, P. Zeng, Z. Li, L. Zhao, X. Fu, *Fuel* **2016**, *175*, 157–163.

[13] Z. Wu, Jing; Shen, Yanming; Liu, Changhou; Wang, Haibin; Geng, Caijun; Zhang, *Catal. Commun.* **2005**, *6*, 633–637.

[14] A. B. Merlo, V. Vetere, J. F. Ruggera, M. L. Casella, *Catal. Commun.* **2009**, *10*, 1665–1669.

[15] Rodiansono, S. Khairi, T. Hara, N. Ichikuni, S. Shimazu, *Catal. Sci. Technol.* **2012**, *2*, 2139.

[16] H. Li, H. Luo, L. Zhuang, W. Dai, M. Qiao, *J. Mol. Catal. A Chem.* **2003**, *203*, 267–275.

[17] R. V. Sharma, U. Das, R. Sammynaiken, A. K. Dalai, *Appl. Catal. A Gen.* **2013**, *454*, 127–136.

[18] J. Kijeński, P. Winiarek, T. Paryjczak, A. Lewicki, A. Mikolajska, *Appl. Catal. A Gen.* **2002**, *233*, 171–182.

[19] B. J. Liaw, S. J. Chiang, S. W. Chen, Y. Z. Chen, *Appl. Catal. A*

WILEY-VCH

*Gen.* **2008**, *346*, 179–188.
[20] S. Sitthisa, D. E. Resasco, *Catal. Letters* **2011**, *141*, 784–791.
[21] W.-S. Lee, Z. Wang, W. Zheng, D. G. Vlachos, A. Bhan, *Catal. Sci. Technol.* **2014**, *4*, 2340.
[22] S. K. Jaatinen, R. S. Karinen, J. S. Lehtonen, *ChemistrySelect* **2016**, *1*, 5363–5373.
[23] P. Panagiotopoulou, D. G. Vlachos, *Appl. Catal. A Gen.* **2014**, *480*, 17–24.
[24] V. Choudhary, A. B. Pinar, S. I. Sandler, D. G. Vlachos, R. F. Lobo, *ACS Catal.* **2011**, *1*, 1724–1728.
[25] M. Hronec, K. Fulajtarová, T. Liptaj, *Appl. Catal. A Gen.* **2012**, *437–438*, 104–111.
[26] M. Hronec, K. Fulajtarová, *Catal. Commun.* **2012**, *24*, 100–104.
[27] V. V. Ordomsky, J.c. Schouten, J. Van Der Schaaf, T. A. Nijhuis, *Appl. Catal. A Gen.* **2013**, *451*, 6–13.
[28] P. Panagiotopoulou, N. Martin, D. G. Vlachos, *J. Mol. Catal. A Chem.* **2014**, *392*, 223–228.
[29] J. J. Musci, A. B. Merlo, M. L. Casella, *Catal. Today* **2017**, *296*, 43–50.
[30] N. S. Biradar, A. A. Hengne, S. N. Birajdar, R. Swami, C. V. Rode, *Org. Process Res. Dev.* **2014**, *18*, 1434–1442.
[31] P. D. Vaidya, V. V. Mahajani, *Ind. Eng. Chem. Res.* **2003**, *42*, 3881–3885.
[32] L.-J. Liu, H.-M. Guo, B. Xue, H. Lou, M. Chen, *RSC Adv.* **2015**, *5*, 66704–66710.
[33] S. K. Jaatinen, R. S. Karinen, J. S. Lehtonen, *ChemistrySelect* **2017**, *2*, 51–60.
[34] F. Rodríguez-Reinoso, *Carbon* **1998**, *36*, 159–175.
[35] J. L. Figueiredo, M. F. R. Pereira, *Catal. Today* **2010**, *150*, 2–7.
[36] E. Lam, J. H. T. Luong, *ACS Catal.* **2014**, *4*, 3393–3410.
[37] P. Serp, B. Machado, *Nanostructured Carbon Materials for Catalysis*, The Royal Society Of Chemistry, Cambridge, **2015**.
[38] Anon., *Calgon Carbon Corporation Investor Presentation*, **2011,** http://phx.corporate-ir.net/External.File?item=UGFyZW50SUQ9ODc0MjV8Q2hpbGRJRD0tMXxUeXBlPTM=&t=1,accessed 18.4.2018.
[39] J. Y. Chen, in *Act. Carbon Fiber Text.* (Ed.: J.Y. Chen), Woodhead Publishing, Duxford, **2017**, pp. 1–18.
[40] L. Prati, D. Bergna, A. Villa, P. Spontoni, C. L. Bianchi, T. Hu, H. Romar, U. Lassi, *Catal. Today* **2018**, *301*, 239–243.
[41] R. Lahti, D. Bergna, H. Romar, T. Hu, A. Comazzi, C. Pirola, C. L. Bianchi, U. Lassi, *Top. Catal.* **2017**, *60*, 1415–1428.
[42] S. H. Y. S. Abdullah, N. H. M. Hanapi, A. Azid, R. Umar, H. Juahir, H. Khatoon, A. Endut, *Renew. Sustain. Energy Rev.* **2017**, *70*, 1040–1051.
[43] M. Ogura, K. Morozumi, S. P. Elangovan, H. Tanada, H. Ando, T. Okubo, *Appl. Catal. B Environ.* **2008**, *77*, 294–299.
[44] X. Z. Yuan, S. M. Fan, S. W. Choi, H. T. Kim, K. B. Lee, *Appl. Energy* **2017**, *195*, 850–860.
[45] M. Amoyal, R. Vidruk-Nehemya, M. V. Landau, M. Herskowitz, *J. Catal.* **2017**, *348*, 29–39.
[46] P. Munnik, P. E. de Jongh, K. P. de Jong, *Chem. Rev.* **2015**, *115*, 6687–6718.
[47] K. Bourikas, C. Kordulis, A. Lycourghiotis, *Catal. Rev. - Sci. Eng.* **2006**, *48*, 363–444.
[48] H. N. Tran, S.-J. You, H.-P. Chao, *Korean J. Chem. Eng.* **2017**, *34*, 1708–1720.
[49] P. Manoj Kumar Reddy, K. Krushnamurty, S. K. Mahammadunnisa, A. Dayamani, C. Subrahmanyam, *Int. J. Environ. Sci. Technol.* **2015**, *12*, 1363–1372.
[50] J. Ma, D. Huang, J. Zou, L. Li, Y. Kong, S. Komarneni, *J. Porous Mater.* **2015**, *22*, 301–311.
[51] S. Brunauer, P. H. Emmett, E. Teller, *J. Am. Chem. Soc.* **1938**, *60*, 309–319.
[52] P. Tarazona, *Phys. Rev. A* **1985**, *32*, 3148–3148.
[53] P. Tarazona, U. M. B. Marconi, R. Evans, *Mol. Phys.* **1987**, *60*, 573–595.
[54] P. A. Lazaridis, S. Karakoulia, A. Delimitis, S. M. Coman, V. I. Parvulescu, K. S. Triantafyllidis, *Catal. Today* **2015**, *257*, 281–290.
[55] N. R. Stuckert, L. Wang, R. T. Yang, *Langmuir* **2010**, *26*, 11963–11971.
[56] C. H. Bartholomew, *Appl. Catal. A Gen.* **2001**, *212*, 17–60.
[57] X. Shen, L. Garces, Y. Ding, K. Laubernds, R. P. Zerger, M. Aindow, E. J. Neth, S. L. Suib, *Appl. Catal. A Gen.* **2008**, *335*, 187–195.
[58] J. H. Bitter, K. P. de Jong, in *Carbon Mater. Catal.* (Eds.: P. Serp, J.L. Figueiredo), John Wiley And Sons, **2008**, pp. 157–176.
[59] M. A. Fraga, E. Jor, M. J. Mendes, M. M. A. Freitas, J. L. Faria, J. L. Figueiredo, *J. Catal.* **2002**, *209*, 355–364.
[60] A. S. Aricò, A. K. Shukla, H. Kim, S. Park, M. Min, V. Antonucci, *Appl. Surf. Sci.* **2001**, *172*, 33–40.
[61] S. Iqbal et al., *ACS Catal.* **2015**, *5*, 5047–5059, see Supporting Information.
[62] A. P. Grosvenor, M. C. Biesinger, R. S. C. Smart, N. S. McIntyre, *Surf. Sci.* **2006**, *600*, 1771–1779.
[63] S. Srivastava, G. C. Jadeja, J. Parikh, *J. Mol. Catal. A Chem.* **2017**, *426*, 244–256.
[64] W. C. Conner, J. L. Falconer, *Chem. Rev.* **1995**, *95*, 759–788.
[65] H. Li, D. Yu, Y. Hu, P. Sun, J. Xia, H. Huang, *Carbon* **2010**, *48*, 4547–4555.
[66] R. Wojcieszak, M. Zieliński, S. Monteverdi, M. M. Bettahar, *J. Colloid Interface Sci.* **2006**, *299*, 238–248.
[67] A. Fuente-Hernández, R. Lee, N. Béland, I. Zamboni, J.-M. Lavoie, *Energies* **2017**, DOI 10.3390/en10030286.
[68] S. Lokras, D. P., N. Kuloor, *Ind. Eng. Chem. Process Des. Dev.* **1970**, *9*, 293–297.
[69] D. Scholz, C. Aellig, I. Hermans, *ChemSusChem* **2014**, *7*, 268–275.
[70] S. Jaatinen, R. Karinen, *Top. Catal.* **2017**, *60*, 1473–1481.
[71] Z. Fu, Z. Wang, W. Lin, W. Song, S. Li, *Appl. Catal. A Gen.* **2017**, *547*, 248–255.
[72] X. Chang, A. F. Liu, B. Cai, J. Y. Luo, H. Pan, Y. B. Huang, *ChemSusChem* **2016**, *9*, 3330–3337.
[73] N. S. Date, N. S. Biradar, R. C. Chikate, C. V. Rode, *ChemistrySelect* **2017**, *2*, 24–32.
[74] L. Wambach, M. Irgang, M. Fischer, *US Pat. 4780552* **1988**.
[75] D. G. Manly, J. P. O'Halloran, *US Pat. 3223714* **1965**.
[76] Rodiansono, S. Khairi, T. Hara, N. Ichikuni, S. Shimazu, *Catal. Sci. Technol.* **2012**, *2*, 2139–2145.

WILEY-VCH

[77] Y. Nakagawa, H. Nakazawa, H. Watanabe, K. Tomishige, *ChemCatChem* **2012**, *4*, 1791–1797.

[78] N. Merat, C. Godawa, A. Gaset, *J. Chem. Technol. Biotechnol.* **1990**, *48*, 145–159.

[79] P. Panagiotopoulou, N. Martin, D. G. Vlachos, *ChemSusChem* **2015**, *8*, 2046–2054.

[80] S. Jaatinen, M. Stekrova, R. Karinen, *J. Porous Mater.* **2017**, DOI 10.1007/s10934-017-0526-7.

[81] R. H. Kottke, *Kirk-Othmer Encycl. Chem. Technol.* **2000**, 259–286.

[82] Anon., https://www.bloomberg.com/quote/XPTUSD:CUR, accessed **27.9.2017**.

[83] S. Srivastava, G. C. Jadeja, J. Parikh, *Chem. Eng. Res. Des.* **2018**, *132*, 313–324.

[84] Z. Fu, Z. Wang, W. Lin, W. Song, *Energy Sources, Part A Recover. Util. Environ. Eff.* **2017**, *39*, 1176–1181.

[85] FprEN 14775:2009 (E), *Solid Biofuels - Determination of Ash Content*, **2005**.

[86] B. M. Babić, S. K. Milonjić, M. J. Polovina, B. V. Kaludierović, *Carbon* **1999**, *37*, 477–481.

[87] F. Raposo, M. A. De La Rubia, R. Borja, *J. Hazard. Mater.* **2009**, *165*, 291–299.

[88] S. Wang, Z. Zhu, *Dye. Pigment.* **2007**, *75*, 306–314.

[89] M. Hirata, N. Kawasaki, T. Nakamura, K. Matsumoto, M. Kabayama, T. Tamura, S. Tanada, *J. Colloid Interface Sci.* **2002**, *254*, 17–22.

[90] G. Bergeret, P. Gallezot, in *Handb. Heteregeneous Catal.* (Eds.: G. Ertl, H. Knözinger, F. Schuth, J. Weitkamp), WILEY-VHC Verlag GmbH & Co. KGaA, Weinheim, **2008**, pp. 738–743.

WILEY-VCH

FULL PAPER

In this work, furfural hydrotreatment was studied over Pt, Ru, and Ni catalysts supported on biomass-based spruce and birch derived activated carbons. Both activated carbons were suitable for catalyst supports. The maximum obtained 2-methylfuran yield of 50% was achieved with 3 wt.% Pt on spruce-based activated carbon. The most important factors affecting 2-methylfuran production were metal dispersion and particle size as well as reaction temperature.

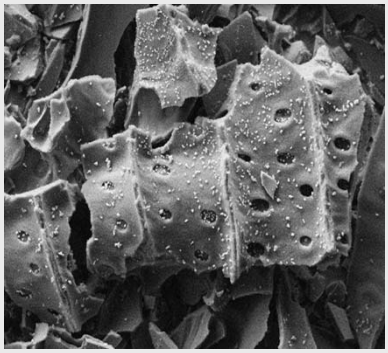

*E. Mäkelä,* R. Lahti, S. Jaatinen, Dr. H. Romar, Dr. T. Hu, Prof. R. L. Puurunen, Prof. U. Lassi and Dr. R. Karinen*

***1-16***

**Study of Ni, Pt and Ru catalysts on wood-based activated carbon supports and their activity in furfural conversion to 2-methylfuran**

WILEY-VCH